2

Conf-9308103--1

LBL-34793
UC-404

Lawrence Berkeley Laboratory
UNIVERSITY OF CALIFORNIA

Materials Sciences Division

Presented at the ASM International Electronic Materials and Processes Conference, San Jose, CA, August 30–September 2, 1993, and to be published in the Proceedings

Research into the Microstructure and Mechanical Behavior of Eutectic Bi-Sn and In-Sn

J.L.F. Goldstein, Z. Mei, and J.W. Morris, Jr.

August 1993

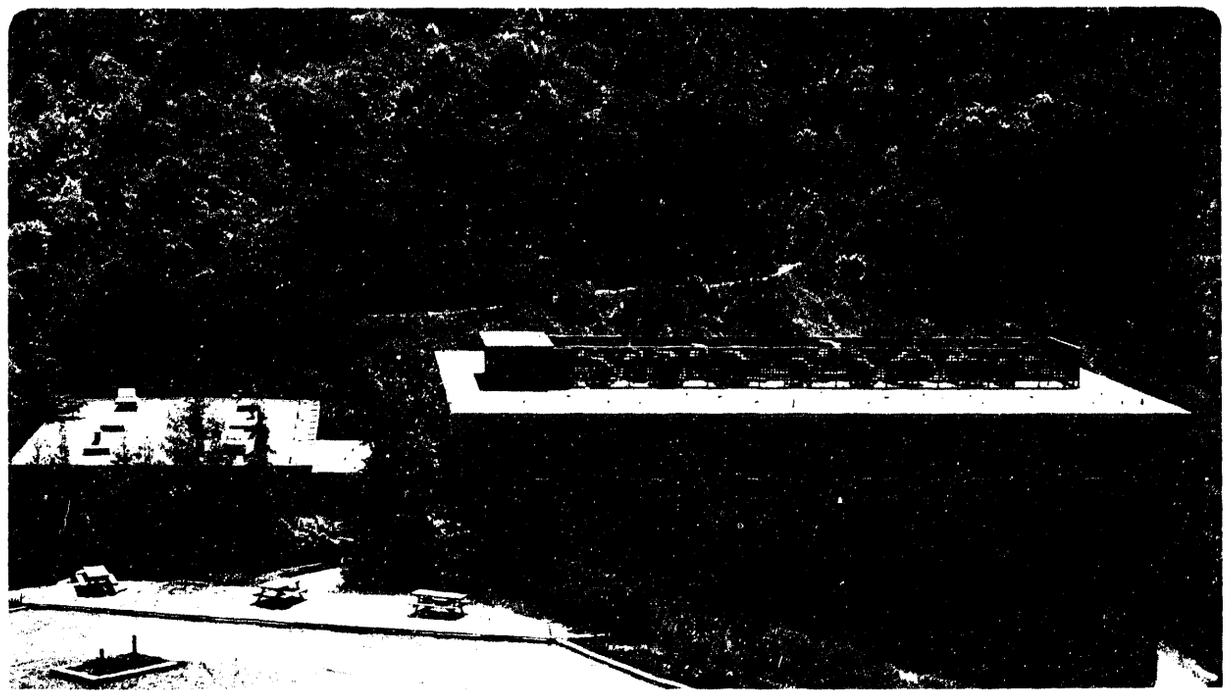

Prepared for the U.S. Department of Energy under Contract Number DE-AC03-76SF00098

DISCLAIMER

LBL 34793

Research Into the Microstructure and Mechanical Behavior of Eutectic Bi-Sn and In-Sn

Julia L. Freer Goldstein, Z. Mei and J. W. Morris, Jr.

Center for Advanced Materials
Materials Sciences Division
Lawrence Berkeley Laboratory
University of California
Berkeley, CA 94720

and

Department of Materials Science and Mineral Engineering
University of California

August 1993

This work was supported by the Director, Office of Energy Research, Office of Basic Energy Science, Materials Science Division of the U.S. Department of Energy under Contract No. DE-AC03-76F00098

Abstract

This manuscript reports on research into two low-melting, lead-free solder alloys, eutectic Bi-Sn and eutectic In-Sn. The microstructures were found to depend on both cooling rate and substrate, with the greatest variability in the In-Sn alloy. The nature of the intermetallic layer formed at the solder-substrate interface depends on both the solder and the substrate (Cu versus Ni). Also, the microstructure of the Bi-Sn can recrystallize during deformation, which is not the case with In-Sn. Data from creep and constant strain rate tests are given for slowly cooled samples. The creep behavior of In-Sn is constant with temperature, but the creep seems to be controlled by the In-rich phase in In-Sn on Cu and by the Sn-rich phase in In-Sn on Ni. Bi-Sn exhibits different creep behavior at temperatures above 40 °C than at 20 °C or lower. Stress-strain curves of Bi-Sn on Cu and In-Sn on Cu are similar, while In-Sn on Ni behaves differently. This is explained is terms of the deformation patterns in the alloys.

EUTECTIC BISMUTH-TIN AND EUTECTIC In-Sn are classified as low-temperature specialty solders. They are used in applications where a low melting point alloy is required, such as in step soldering or when components in an assembly are sensitive to temperature. Bi-Sn has also been used for hermetic seals. Recently, interest in these alloys has been heightened by threats of a congressional ban on lead in microelectronics. If such a ban were implemented, alternative solders would be needed. Although neither of the alloys in this study would be used as a direct substitute for eutectic Sn-Pb, a suitable substitute is likely to contain some combination of Sn, Bi and In and therefore it is timely to study alloys of these metals.

Research on the mechanical behavior of Bi-Sn and In-Sn alloys has been limited. Several articles present data on mechanical properties of various alloys and show Bi-Sn to be stronger and more creep resistant than In-Sn or Sn-Pb, but to be much less ductile and have a lower fatigue life [1-3]. In-Sn alloys have particularly low strength, high ductility, and correspondingly low creep resistance. Frenkel [4] studied creep of the pure metals and found activation energies of 0.91 eV for polycrystalline tin and 0.72 eV for polycrystalline indium.

According to the In-Sn [5] and Bi-Sn [6] phase diagrams, the eutectic temperatures are 120°C and 138°C, respectively. Bi-Sn is a simple eutectic, consisting of tin and bismuth terminal solid solutions (see Figure 1). The solubility of Bi in Sn is 21 weight percent at the eutectic temperature and decreases to about 2 percent at room temperature. The maximum solubility of Sn in Bi is 0.1 weight percent. The In-Sn binary phase diagram is shown in Figure 2. The eutectic, with a melting point of 120 °C, is composed of two intermediate phases, the Sn-rich γ phase and the In-rich β phase. Both the γ and β phases are relatively soft and ductile and have wide solubility ranges, in contrast to the behavior expected for ordered intermetallics. The composition of the γ phase of the eutectic does not change much as the alloy is cooled. The composition of the β phase, however, varies from 44 atomic percent at the eutectic temperature to 30 atomic percent at 25 °C.

The purpose of the studies reported here was to gain an understanding of the deformation of In-Sn and Bi-Sn solders by examining the mechanical properties and microstructure in parallel. In particular, the effects of variables such as

cooling rate and substrate on the microstructure and the dependence of stress, strain rate and test temperature on the mechanical behavior were investigated.

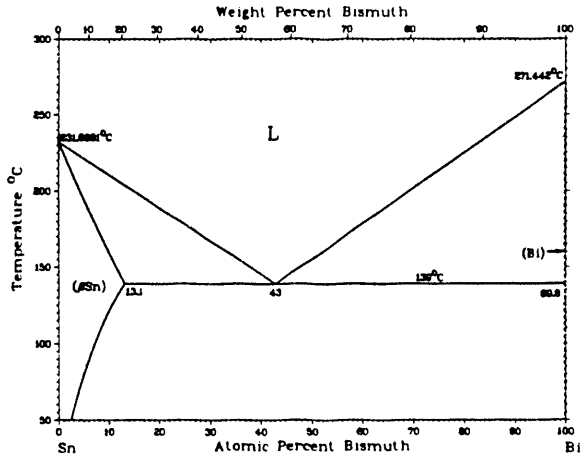

Fig. 1 - Bi-Sn phase diagram, from ref. 6.

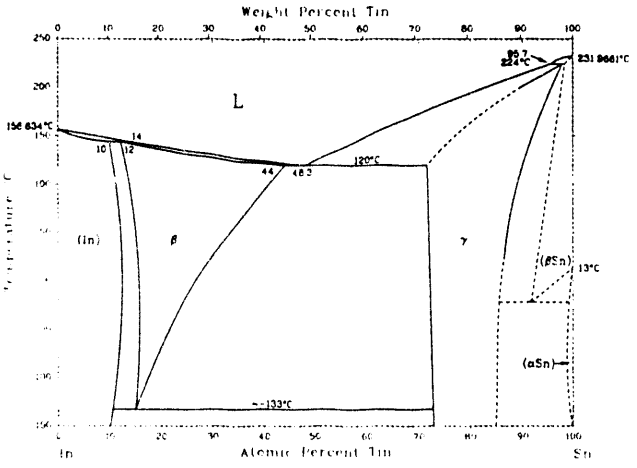

Fig. 2 - In-Sn phase diagram, from ref. 5.

Experimental Procedure

Copper is a common substrate to which most solder alloys are bonded. However, it has been observed [7] that poor quality solder joints result when soldering In-Sn directly to a copper substrate, due to rapid diffusion of Cu into the In-rich alloy. For this reason, a layer of Ni is generally used as a diffusion barrier. Therefore, three solder/substrate combinations were used in this research: Bi-Sn on Cu, In-Sn on Cu and In-Sn on Ni.

Two types of samples were used for mechanical testing and microstructural analysis: modified double-lap shear samples (see Figure 3), which were cooled very slowly, and nine-pad arrays (see Figure 4), which were cooled rapidly.

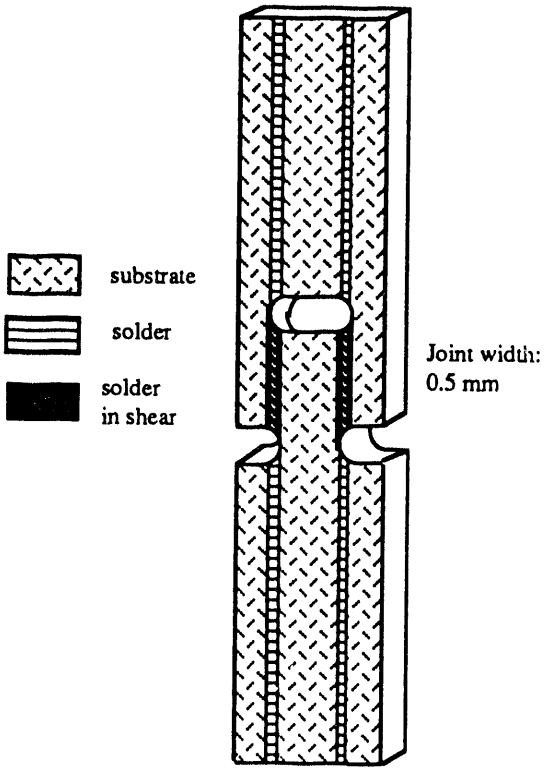

Fig. 3 - Modified double-lap shear sample.

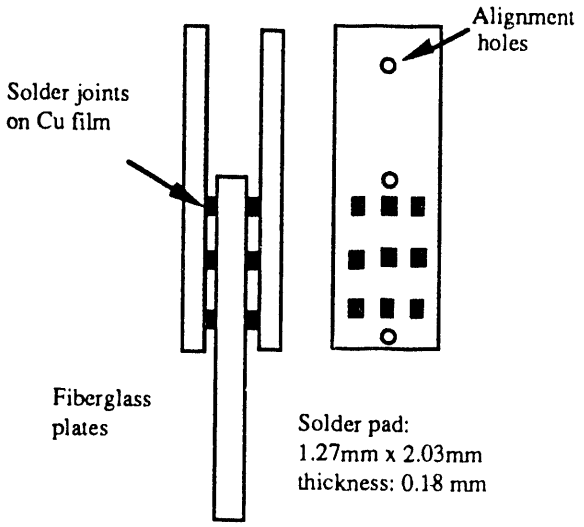

Fig. 4 - Nine-pad array sample.

The modified double-lap shear samples consist of three Cu blocks bonded together by two 0.5 mm wide (0.020 inch) solder joints. For the In-Sn on Ni, the Cu blocks were plated with about 8 μm of Ni before assembly. Details of the method used to manufacture the samples have been published elsewhere [8]. The design of these samples is such that when the entire sample is pulled in tension, the central gage region is deformed in shear.

The FR4 epoxy boards were plated with Cu before applying solder paste to produce the nine-pad array samples. In-Sn on Ni samples were not made in this configuration. Details of the sample preparation procedure appear in a previous publication [9].

The information on deformed microstructures and mechanical testing will focus on the slowly cooled samples. The samples were tested both at constant load (creep) and at constant strain rate. Tests were done at temperatures between 0 and 75 °C, which correspond to homologous temperatures of over 65 percent and are thus considered high temperature tests. Elevated temperature tests were run by submerging the sample into a heated silicone oil bath and allowing the temperature to stabilize for 30 to 60 minutes before starting the test. The creep tests were run until the samples reached the tertiary creep region. Applied shear stresses ranged from 1 to 12 MPa for In-Sn samples and from 7 to 76 MPa for Bi-Sn samples.

Constant strain rate tests were run until an arbitrary total strain was reached, at strain rates ranging from $2x10^{-4}$ to $8x10^{-4}$ mm/mm/sec for both alloys. In all cases, tests were usually stopped before fracture of the samples.

Creep data is presented in the form of log-log plots of steady-state strain rate versus applied stress and is analyzed in terms of the power law creep equation, shown below, which describes the effect of stress and temperature on the steady-state creep rate:

$$d\gamma/dt = A\,\tau^n \exp(-Q/kT). \qquad (1)$$

The pre-exponential factor, A, is a microstructural parameter roughly independent of stress and temperature, n is the stress exponent, and Q is the apparent activation energy for creep. Evaluation of n and Q can often help identify the dominant mechanism of creep deformation for a given system and range of experimental conditions. The activation energy for creep of each type of sample was determined by using multivariable linear regression to fit all stress, temperature and strain rate data to a single equation of the form:

$$Y = m_1x_1 + m_2x_2 + b \qquad (2)$$

In this case, $Y = \ln(d\gamma/dt)$, $x_1 = \ln(\tau)$, $x_2 = 1/T$, $m_1 = n$, $m_2 = -Q/k$, and $b = \ln(A)$.

Some In-Sn samples were aged at 81 °C (0.9 T_m) to investigate the effect of aging on the microstructure and mechanical behavior and to better observe the intermetallic compounds formed at the interface between the solder and the substrate.

Results and Discussion

Untested Microstructures. The untested as-cast microstructures of the two alloys differ considerably. Bi-Sn has what can be called a complex regular microstructure. The two phases are apparently arranged in alternating plates, but the plates are not flat, resulting in a microstructure with complicated patterns. This morphology exists for both slowly cooled samples (Figure 5) and rapidly cooled samples (Figure 6). In the slowly cooled samples, the microstructure consists of cells, with similar lamellar orientation within each cell. The cellular structure is absent in the more uniform microstructure of the rapidly cooled samples. In the slowly cooled samples, isolated islands of Sn dendrites or faceted Bi particles are observed. The decrease in solid solubility of Bi in Sn as the alloy is cooled causes Bi precipitates to form within the Sn-rich regions of the eutectic. This precipitation can be seen easily within the Sn dendrites in Figure 5b.

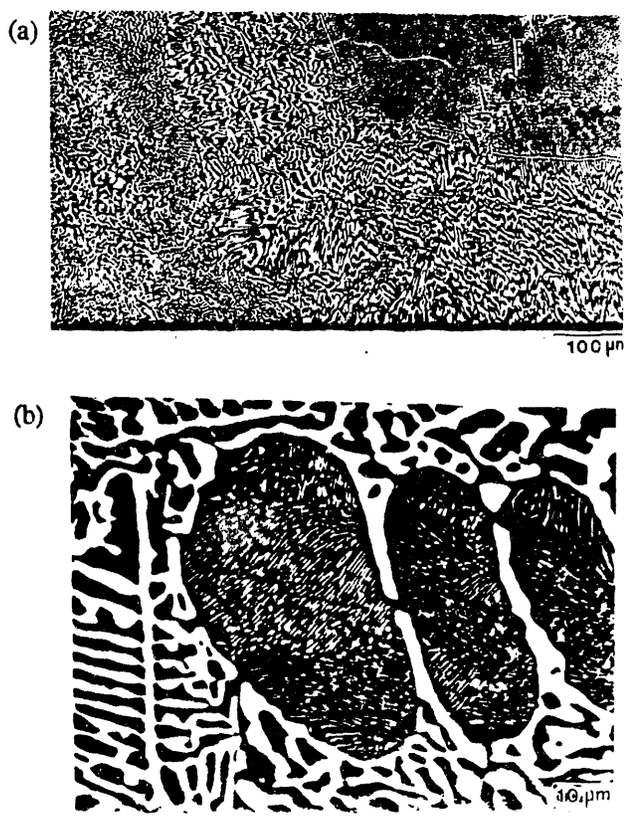

Fig. 5 - Optical micrographs of slowly cooled Bi-Sn.

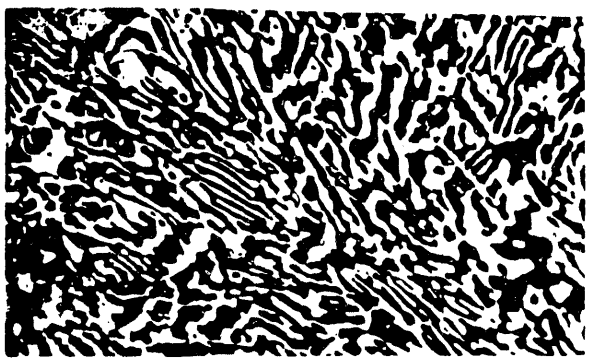

Fig. 6 - Optical micrographs of rapidly cooled Bi-Sn.

The microstructure of the slowly cooled eutectic In-Sn depends strongly on the substrate. In-Sn on Cu (Figure 7a) has an irregular microstructure, the scale and morphology of which varies throughout the joint. No well-developed lamellar structure exists, although lamellae form in isolated regions. Many large dendrites of the Sn-rich γ phase are also observed. The γ phase is discontinuous, implying that the γ phase regions are imbedded in a matrix of the β phase. The microstructure of In-Sn on Ni is quite different, as can be seen in Figure 7b. The eutectic phases are arranged in lamellar colonies, in a microstructure which is much more uniform. No large regions of either phase are present, and neither phase seems to form a continuous matrix. The rapidly cooled samples have a different microstructure altogether. The morphology is equiaxed and uniform throughout the sample. An example appears in Figure 8.

Aging has no visible effect on the microstructure of slowly cooled In-Sn on Cu. In-Sn on Ni samples aged for two months at 81 °C show remarkable microstructural changes. No trace of the as-cast colony microstructure remains. Instead, the microstructure throughout the joint has evolved into what appear to be islands of γ phase in a matrix of the β phase, similar to the situation in In-Sn on Cu. The micrograph in Figure 9 is of an In-Sn on Ni sample after aging, which illustrates the dramatic effect of aging on the microstructure.

The bond between the solder and substrate is formed by intermetallic compounds at the interface. The intermetallic layer formed between Bi-Sn and Cu is about 1 μm thick and contains Cu and Sn. It is too thin to be seen in the micrographs shown, but is visible by SEM. In the Sn-Pb/Cu system, Cu_3Sn and Cu_6Sn_5 intermetallics form [10]. Intermetallic particles exist within the Bi-Sn solder in the form of hexagonal rods, a known morphology for Cu_6Sn_5.

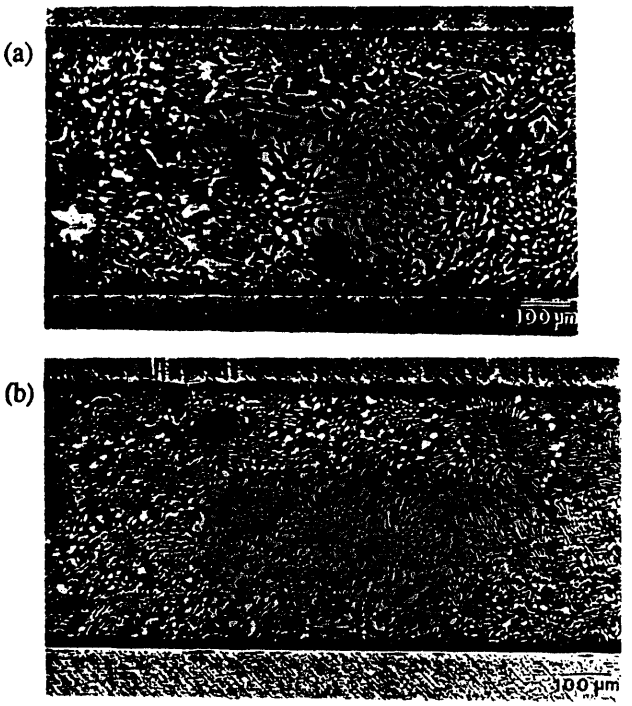

Fig. 7 - Optical micrographs of slowly cooled In-Sn on (a) Cu and (b) Ni substrates.

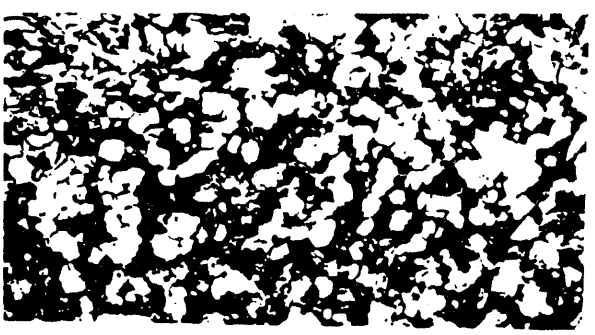

Fig. 8 - Optical micrograph of rapidly cooled In-Sn.

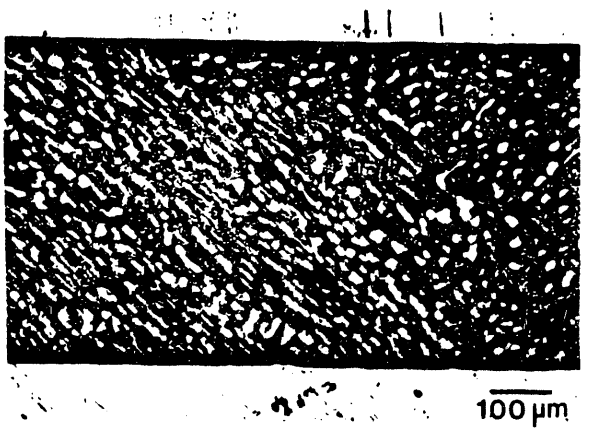

Fig. 9 - Optical micrograph of aged In-Sn on Ni.

Formation of a Cu_6Sn_5 intermetallic layer in the Bi-Sn/Cu system has been previously observed [1], and its existence both at the interface and within the Bi-Sn solder has been confirmed by energy dispersive spectroscopy on the SEM. The intermetallic layer at the solder-substrate interface naturally varies with substrate. In-Sn on Cu forms ternary intermetallics. These have been discussed in an earlier paper [8]. The intermetallic region is actually composed of two layers, with a layer of Cu_2In_3Sn on the solder side and a layer of $Cu_2(Sn,In)$ on the Cu side of the interface. Similarly, samples on Ni develop a ternary In-Sn-Ni intermetallic layer, though its stoichiometry has not been determined.

Tested Microstructures. Deformation in all samples begins at the corners where stress and strain are concentrated, but the manner in which it spreads can vary. In-Sn on Ni samples show surface relief throughout the width and length of the sample, though the most severe deformation is often within particular colonies. The deformation pattern for In-Sn on Cu is much more concentrated, following in a band along the length of the joint. These differences are illustrated in Figures 10 and 11. For all samples, some minimum amount of strain is required to induce visible surface relief.

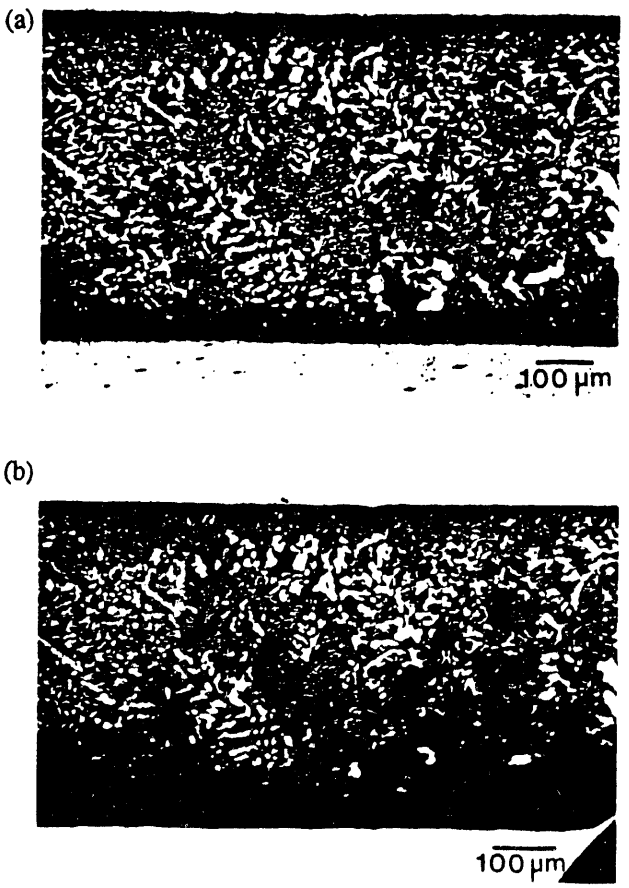

Fig. 10. - Optical micrographs of slowly cooled In-Sn on Cu, (a) before and (b) after testing.

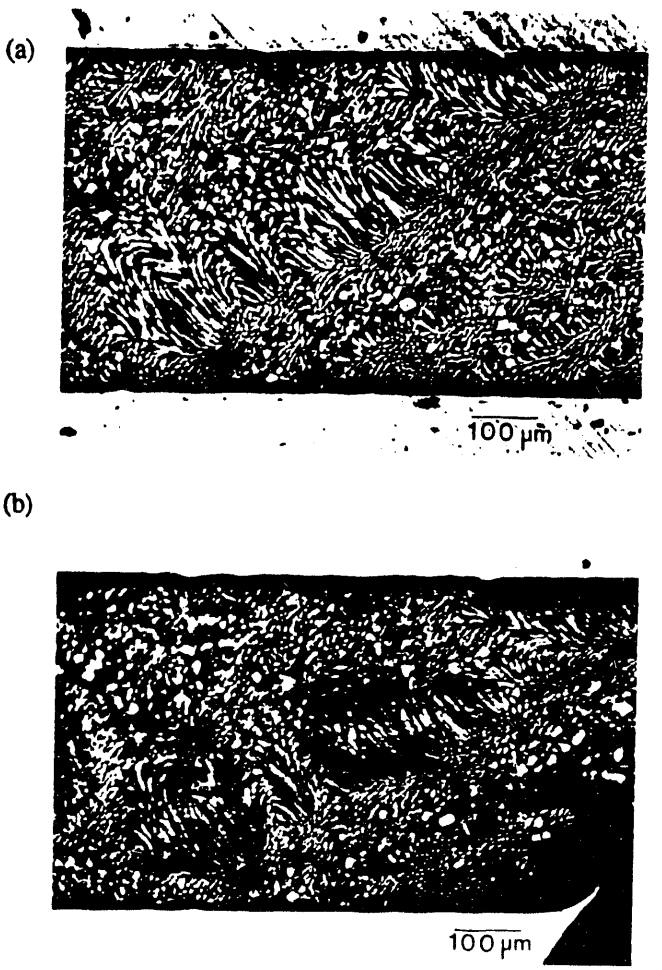

Fig. 11. - Optical micrographs of slowly cooled In-Sn on Ni, (a) before and (b) after testing.

Bi-Sn also exhibits deformation concentrated in a band along the length of the joint, but it also experiences microstructural changes under certain experimental conditions. The micrograph in Figure 12 shows a Bi-Sn sample as-tested and after repolishing to reveal the tested microstructure. A narrow band of material in the most highly deformed region of the sample has a distinctly different microstructure from the rest of the joint. It appears to have been reconfigured in some manner. The high magnification micrographs in Figure 13 illustrate this region in more detail. This localized change in the microstructure can also occur during constant strain rate tests.

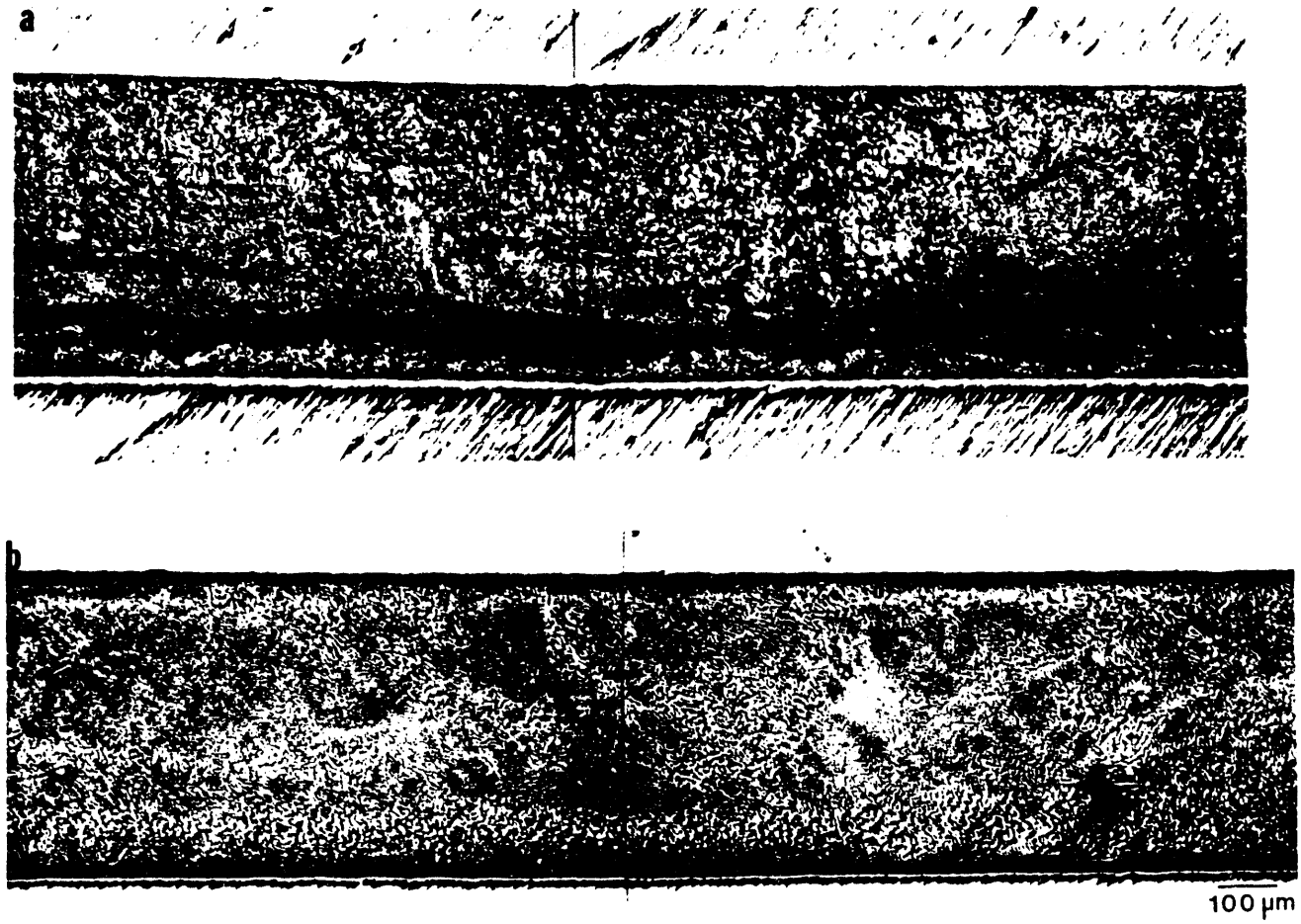

Fig. 12 - Optical micrographs of tested Bi-Sn sample, (a) as-tested and (b) repolished to reveal microstructure.

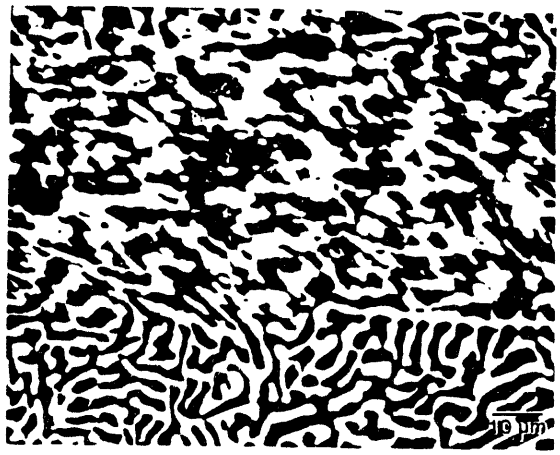

Fig. 13 - Optical micrograph of tested and repolished Bi-Sn sample.

Microstructural changes in Bi-Sn always occur in the same location in the samples, and have been observed in samples tested under a wide range of stress and strain rate conditions. However, this behavior did not occur in every sample tested. An analysis of 12 tested Bi-Sn samples showed a definite correlation between total shear strain and microstructural reconfiguration. A minimum shear strain of between 20 and 30 percent was required to cause a distinct change.

The question of whether it is appropriate to label the microstructural changes which are observed in deformed Bi-Sn as recrystallization is complicated. In order to address this question it is useful to consider two mechanisms for dynamic recrystallization. The first is a nucleation and growth mechanism, which is used to describe both static and dynamic recrystallization. Nucleation and growth of recrystallized grains results in an equiaxed microstructure, similar to that previously observed in tested Sn-Pb joints [11]. Another mechanism used to explain dynamic recrystallization is grain boundary migration and/or bulging. Grain boundaries can migrate or bulge out, leaving behind regions of dislocation-free material without creating new grains. This results in a structure that is not equiaxed, but has a texture similar to the original structure. This model better fits the observed behavior of Bi-Sn. However, instead of

grain boundaries it is inter-phase boundaries which migrate. In this context, it seems appropriate to label the microstructural changes observed in Bi-Sn as dynamic recrystallization.

The type of microstructural changes that occur in Bi-Sn have not been observed in In-Sn. The microstructure of In-Sn appears to be unaffected by testing. This is probably due to the extreme softness and ductility of the alloy. Recovery occurs to such a great extent during deformation that the alloy never builds up sufficient driving force to cause inter-phase boundary migration or nucleation of new grains.

Creep Behavior. Log-log plots of steady-state strain rate versus applied stress for slowly cooled In-Sn on Cu and In-Sn on Ni appear in Figure 14. The data fit very well to straight lines for all temperatures tested. Stress exponents are near 3 for samples on Cu and close to 5 for samples on Ni and are relatively constant with temperature. Due to the difference in stress exponents, the Cu and Ni data lines at a given temperature will cross. Therefore, at high stresses the creep rate of Ni samples is generally higher than for Cu samples at the same stress, whereas at lower stresses the opposite is true. Activation energies for creep of the two systems calculated using Eq. 2 resulted in Q = 0.73 eV for In-Sn on Cu and Q = 1.04 eV for In-Sn on Ni. For comparison, literature values for bulk self-diffusion activation energies of In and Sn are 0.78 [12] and 1.08 eV [13,14], respectively. Activation energies for grain boundary diffusion are much lower, implying that grain boundary sliding is not dominant in either system.

By examining the microstructures and activation energies for creep of In-Sn on Cu and In-Sn on Ni the following conclusions were drawn. Since the microstructure of In-Sn on Cu appears to consist of γ phase regions in a β phase matrix, it is reasonable to presume that the β phase domi nates the creep deformation. The islands of γ phase are discontinuous and do not control the deformation but are swept along in the flow of the β phase. For In-Sn on Ni the data strongly suggest that the Sn-rich γ phase is controlling the creep behavior. In the lamellar eutectic microstructure the two phases are strongly coupled, and the deformation is dominated by the harder phase. Creep controlled by the Sn-rich phase is also supported by creep data on pure Sn [15], in which the authors found an activation energy for creep of 1.0 eV, similar to the activation energy for creep of In-Sn on Ni. Creep testing of an aged In-Sn on Ni sample at 65 °C gave a stress exponent of 3.4. The strain rate versus stress data follows the same curve as the data for In-Sn on Cu samples at the same test temperature. This makes sense, since the microstructure of aged In-Sn on Ni consists of γ phases

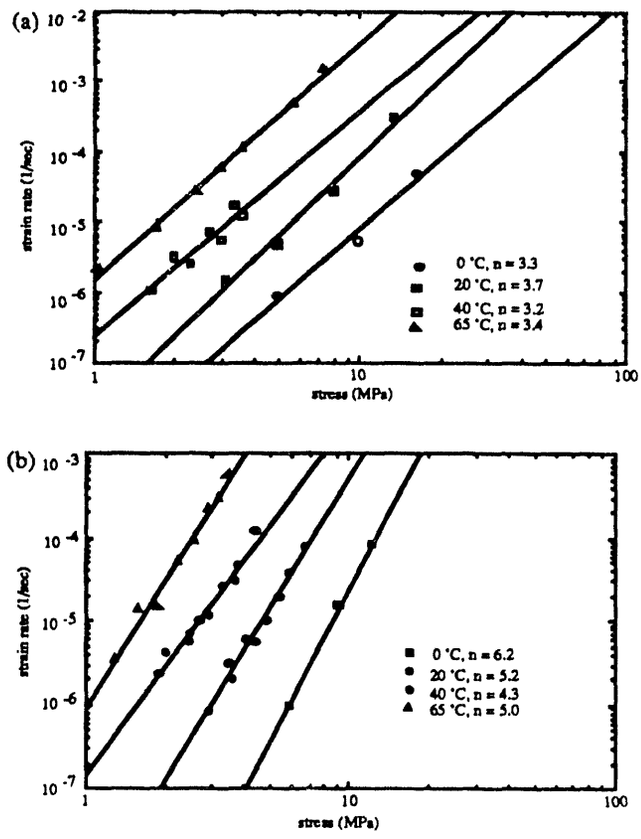

Fig. 14 - Creep data for (a) In-Sn on Cu and (b) In-Sn on Ni.

imbedded in a matrix of the β phase, which should produce creep controlled by the β phase, just as for In-Sn on Cu. The creep behavior of In-Sn on Cu does not change with aging.

The creep behavior of Bi-Sn changes with temperature, as can be seen from the plot of steady-state strain rate versus applied stress in Figure 15. At 65 and 75 °C, a single value of the stress exponent n, between 4 and 5, characterizes the steady-state creep behavior. However, at lower temperatures (0 to 20 °C) the data do not fit well on a single line, but split into low stress and high stress regimes. The low stress region exhibits an n value near three, similar to the n values for In-Sn. The stress exponent in the high stress region is quite high, greater than 6. Interestingly enough, the stress exponents at high temperature are between these two values.

The shape of the Bi-Sn creep curves in the primary and steady-state regions also depends on the testing temperature. At temperatures of 0 and 20 °C, the creep curves appear like the one shown in Figure 16a. There is a distinct primary creep region and then a smooth transition into steady-state creep. The steady-state creep region is well-defined, with a perfectly constant slope. In contrast, the creep curves at temperatures of 65 and 75 °C are very rough. The example

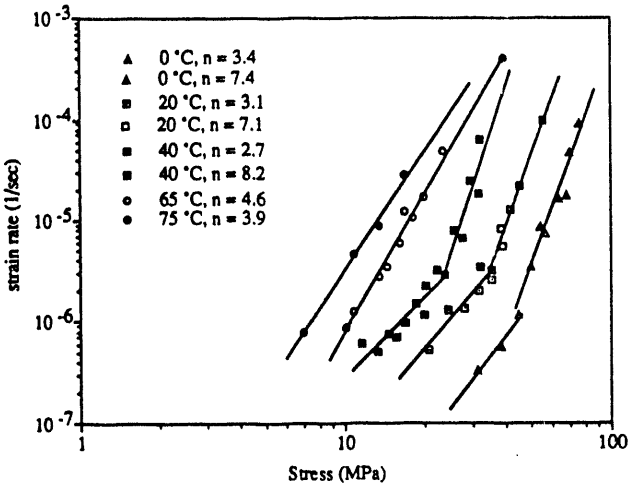

Fig. 15 - Creep data for Bi-Sn on Cu.

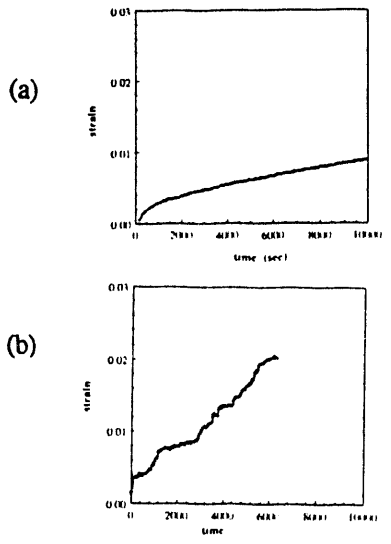

Fig. 16 - Creep curves for Bi-Sn at (a) 20 °C and (b) 65 °C.

of a 65 °C test in Figure 16b shows that there is no prolonged region of constant strain rate. The strain rate oscillates, and so the steady-state creep region is defined by a period during which the average creep rate is constant, before it begins to rise rapidly during tertiary creep. There may be a primary creep region for this sample, but it is obscured by the roughness of the data. The creep behavior for the other test temperature used, 40 °C, falls between that observed at higher or lower temperatures. When the shape of the creep curves and the variation of stress exponent are considered together, it appears as though two mechanisms are competing for control of the deformation at very high temperatures, whereas at lower temperatures one mechanism controls at low stresses and the other at high stresses. The stress at which this break occurs depends on temperature.

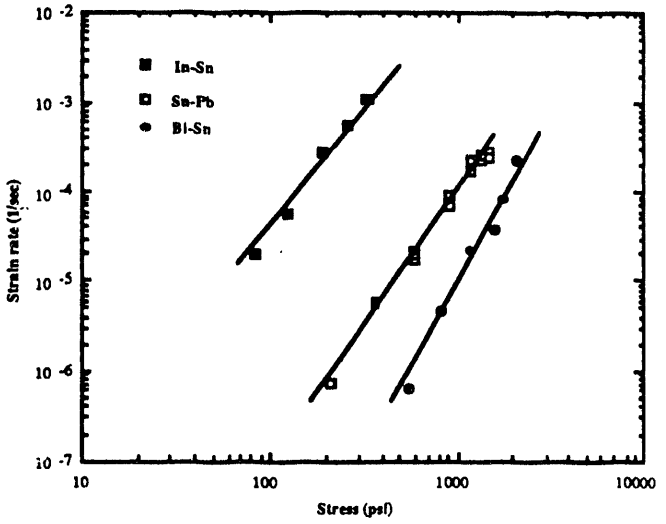

Fig. 17 - Creep data for In-Sn, Bi-Sn and Sn-Pb at 65 °C.

It is useful to compare the creep resistance of In-Sn and Bi-Sn to that of Sn-Pb. An alloy with high creep resistance will have a relatively low steady-state strain rate at a given applied stress and test temperature. Data at 65 °C for all three alloys is plotted in Figure 17. It can be seen that Bi-Sn is slightly more creep resistant than Sn-Pb, while the creep resistance of In-Sn is extremely low.

Stress-Strain Behavior. The stress-strain curves for Bi-Sn (Figure 18) and for In-Sn on Cu (Figure 19) are qualitatively similar. The stress rises quickly to a peak and then decays logarithmically. However, Bi-Sn experiences much higher peak stresses and slower decay rates (longer time to fall to a given fraction of the peak stress) than In-Sn. Figure 19 also shows stress-strain curves for In-Sn on Ni. For these samples the stress does not decay but remains almost constant after reaching the peak.

The rapid decay in flow stress of the Bi-Sn and In-Sn on Cu can be explained in two ways. The non-uniform deformation mentioned earlier has the consequence that the entire sample is not experiencing the strain measured by the strain gage, which registers overall displacement. Therefore, the local strain rate is actually higher than that measured by differentiating "bulk" strain with respect to time. The stress is also distributed over a smaller area than assumed, so that the calculated stress is too low. This implies that the stress drop is not really as steep as the plots in Figures 19 and 20 indicate. However, this probably does not account for all of the stress drop. A second reason for a decrease in flow stress is microstructural softening, since recovery is expected to be significant at the testing temperatures used. Since the concentration of deformation cannot be quantified, it is

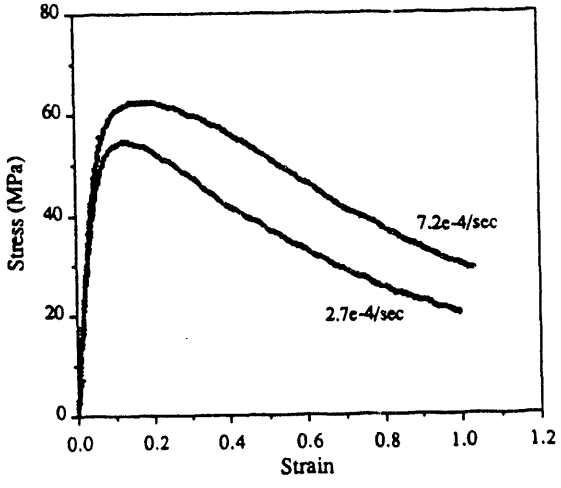

Fig. 18 - Stress strain curves for Bi-Sn at 40 °C.

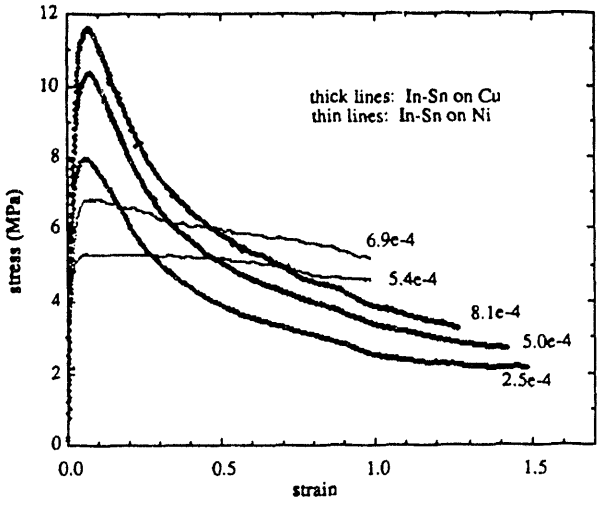

Fig. 19 - Stress-strain curves for In-Sn on Cu and on Ni at 40 °C.

difficult to tell how much of the apparent stress drop is due to this concentration and how much to microstructural softening.

The In-Sn on Ni samples exhibit neither severe deformation concentrations nor dramatic drops in the flow stress during stress-strain tests. It appears that with the geometrical factors eliminated, the slight decrease in stress during testing is due only to microstructural softening. This supports the idea that stress and strain concentrations are responsible for much of the stress decay observed in Bi-Sn and In-Sn on Cu.

There is an important connection between the creep and constant strain rate behavior. In the plots in Figure 20, creep data is plotted as steady-state strain rate versus applied stress and stress-strain data is presented as applied strain rate versus peak stress. It is apparent from the plots that the data on In-Sn from the two types of tests lie on the same line at a given temperature. This implies that the shear strength at a given strain rate can be predicted from creep data. This can be useful, since creep data is generally easier to generate for a wide range of stresses and strain rates.

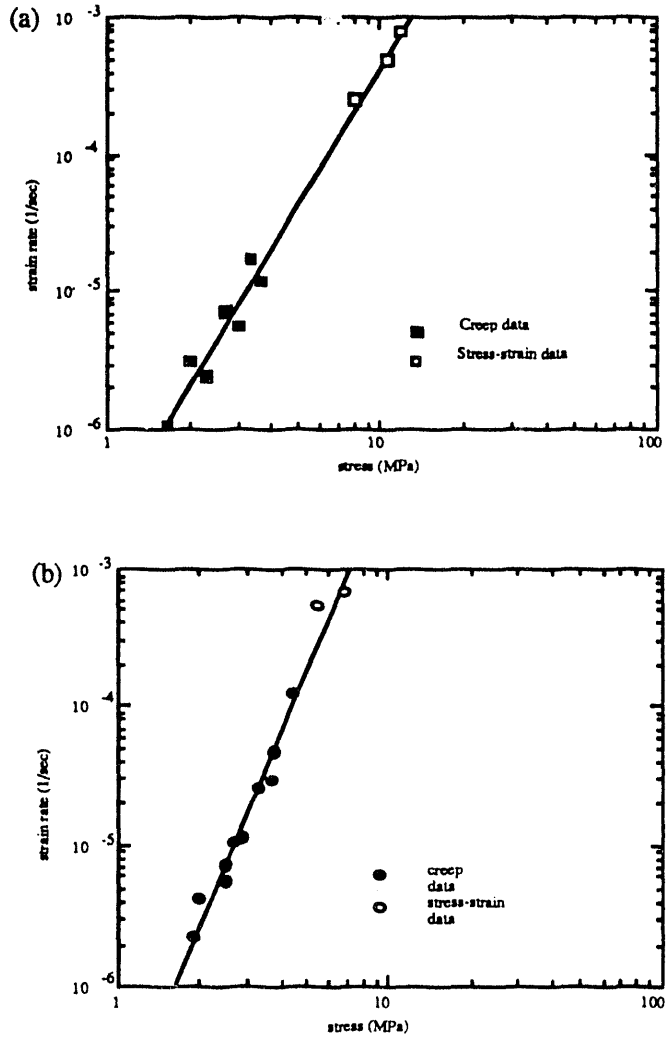

Fig. 20 - Connection between creep and stress-strain data for (a) In-Sn on Cu and (b) In-Sn on Ni at 40 °C.

Conclusions

This research has demonstrated the known fact that the microstructure of an alloy depends not only on its composition but on processing variables such as cooling rate and substrate. Also, aging can dramatically change the microstructure, as seen by the example of slowly cooled In-Sn on Ni. These factors need to be considered in solder joint

design. The microstructure also affects the mechanical behavior. The mechanism of creep of In-Sn changes with substrate, and aging of In-Sn on Ni causes the creep behavior to switch to that of In-Sn on Cu. It is not clear from the results presented here whether control of creep deformation by the γ phase or the β phase is more desirable. The change of creep mechanism of Bi-Sn with temperature is important, since it implies that accelerated high temperature testing of this alloy cannot predict the behavior at ambient temperature.

Acknowledgment

The solder alloys used in this study, Indalloys 1E and 281, were provided by the Indium Corporation of America. This work was supported by the Director, Office of Energy Research, Office of Basic Energy Sciences, U. S. Dept. of Energy, under Contract No. DE-AC03-76SF00098.

References

1 W. J. Tomlinson and I. Collier, J. Mater. Sci., 22, 1835-39 (1987).

2 K. S. Dogra, Brazing and Soldering, 9, 28-30 (1985).

3 R. N. Wild, "Some Fatigue Properties of Solders and Solder Joints," IBM Report no. 74Z00481, Oswego, NY (1975).

4 Robert E. Frenkel, M. S. Thesis, University of California, Berkeley, CA (1954).

5 C. E. T. White and H. Okamoto, "Phase Diagrams of Indium Alloys and Their Engineering Applications," p. 255, Indium Corporation of America, Utica, NY and ASM Intl., Materials Park, OH (1992).

6 M. Hansen and K. Anderko, "Constitution of Binary Alloys," p. 336, Mc-Graw-Hill, New York, NY (1958).

7 C.E. T. White and G. P. Evans, Research and Development, 28, 88-90 (1986).

8 J. L. Freer and J. W. Morris, Jr., J. Electon. Mater., 1992, 21, 647-52 (1992).

9 Z. Mei, M. C. Shine, T.S. E. Summers, and J. W. Morris, Jr., J. Electon. Mater., 20, 599-608 (1991).

10 D. Frear, D. Grivas, and J. W. Morris, Jr., J. Electron. Mater., 16, 181-86 (1987).

11 D. Tribula, D. Grivas, D. Frear, and J.W. Morris, Jr., J. Electr. Packaging, 111, 83-89 (1989).

12 R. E. Eckert and H. J. Drickamer, J. Chem. Phys., 20, 13-17 (1952).

13 J. D. Meakin and E. Klokholm, Trans. Met. Soc. AIME, 218, 463-66 (1960).

14 C. Coston and N. H. Nachtreib, J. Phys. Chem., 68, 2219-29 (1964).

15 F. A. Mohamed, K. L. Murty and J. W. Morris, Jr., Metall. Trans, 4, 935-40 (1973).

List of Figures

END

DATE
FILMED
2/2/94